

Available online at www.sciencedirect.com

ScienceDirect

www.elsevier.com/locate/jes

JES
JOURNAL OF
ENVIRONMENTAL
SCIENCES
www.jesc.ac.cn

Effective adsorption of sulfamethoxazole, bisphenol A and methyl orange on nanoporous carbon derived from metal-organic frameworks

Xiaona Li¹, Hui Yuan¹, Xie Quan^{1,*}, Shuo Chen¹, Shijie You²

1. Key Laboratory of Industrial Ecology and Environmental Engineering (Ministry of Education), School of Environmental Science and Technology, Dalian University of Technology, Ling gong Road 2, Dalian 116024, China

2. State Key Laboratory of Urban Water Resource and Environment, School of Environment, Harbin Institute of Technology, Harbin 150090, China

ARTICLE INFO

Article history:

Received 15 July 2017

Revised 25 October 2017

Accepted 26 October 2017

Available online 10 November 2017

Keywords:

Nanoporous carbon

MOFs

Adsorption

Sulfamethoxazole

Bisphenol A

Methyl orange

ABSTRACT

Nanoporous carbons (NPCs) derived from metal-organic frameworks (MOFs) are attracting increasing attention in many areas by virtue of their high specific surface area, large pore volume and unique porosity. The present work reports the preparation of an NPC with high surface area (1731 m²/g) and pore volume (1.68 cm³/g) by direct carbonization of MOF-5. We examined the adsorption of three typical contaminants from aqueous solutions, i.e., sulfamethoxazole (SMX), bisphenol A (BPA) and methyl orange (MO), by using the as-prepared NPC. The results demonstrated that NPC could adsorb the contaminants effectively, with adsorption capacity (q_m) of 625 mg/g (SMX), 757 mg/g (BPA) and 872 mg/g (MO), respectively. These values were approximately 1.0–3.2 times higher than those obtained for single-walled carbon nanotubes (SWCNTs) and commercial powder active carbon (PAC) under the same conditions. With its high surface area and unique meso/macropore structure, the enhanced adsorption of NPC most likely originates from the cooperative interaction of a pore-filling mechanism, electrostatic interaction, and hydrogen bonding. In particular, the pH value has a crucial impact on adsorption, suggesting the significant contribution of electrostatic interaction between NPC and the contaminants. This study provides a proof-of-concept demonstration of MOF-derived nanoporous carbons as effective adsorbents of contaminants for water treatment.

© 2017 The Research Center for Eco-Environmental Sciences, Chinese Academy of Sciences.

Published by Elsevier B.V.

Introduction

Nanoporous carbon (NPC) materials have received growing interest in a variety of applications such as super-capacitors (Prehal et al., 2017), gas storage (Yang et al., 2012; Kim and Park, 2007) and catalyst supports (Seo et al., 2000). It would be also highly desirable to develop NPC materials with unique porous structure and high surface area for adsorption of environmental contaminants (Lee et al., 2014; Ji et al., 2010). Generally, NPC materials can be prepared by several routes including chemical

vapor decomposition, templating synthesis as well as chemical- or physical-activation. Template-based synthesis has been considered to be an effective approach, as it allows designing and manipulating the porous structure of NPC during preparation (Lim et al., 2012). Therefore, a particular emphasis should be placed on the selection of suitable precursors to obtain the expected functionalized NPC materials.

Metal-organic frameworks (MOFs) are inorganic-organic hybrids with tunable pore sizes and functionalities (Sneddon et al.,

* Corresponding author. E-mail address: quanxie@dlut.edu.cn (Xie Quan).

2014). As porous structured materials, MOFs are promising precursors for NPC fabrication due to their significant carbon contents (Chaikittisilp et al., 2013). Prior studies reported that MOF-derived NPC could have a high surface area and large pore volume (Gadipelli et al., 2015; Hu et al., 2010), which are the two most essential factors that determine the adsorption capacity of NPC. Meanwhile, the unique porosity of MOF-derived NPC is another advantage (Chaikittisilp et al., 2012), which makes it possible to separate contaminants selectively from aqueous solution (Li et al., 2016).

Contaminant removal by adsorption is an efficient method due to advantages such as simple operation, high performance and low cost. The adsorption of organic micropollutants such as pesticides and medicines has been studied using carbon-based adsorbents, nanoporous polymers, organoclays and various other porous materials (Alsaiee et al., 2016; Byun et al., 2016). Activated carbon has been used as the most efficient adsorbent; however, it is flammable and difficult to regenerate (Patel et al., 2009). In comparison, MOF-derived NPC, with unique pore sizes and shapes combined with target-specific functionality, have exhibited their potential for adsorption of environmental pollutants (Lee et al., 2014; Ji et al., 2010).

To the best of our knowledge, the limited reports on removal of organic pollutants by using MOF-derived NPC materials have only achieved unsatisfactory results. Lee et al. examined the separation of a typical dye (methylene blue) by a Fe-MIL-88 derived NPC (Lee et al., 2014). Despite the detailed characterization of the prepared adsorbent, the adsorption capacity (83.9 mg/g) was much lower than that of activated carbon (Bedin et al., 2016; Uner et al., 2016), which may greatly limit its practical application. Therefore, it will be of particular importance to develop more efficient MOF-derived NPC for enhanced adsorption of organic pollutants in practical water treatment.

To address these challenging problems, we in this study prepared a NPC material by direct carbonization of MOF-5, and investigated the adsorption performance towards three typical pollutants, sulfamethoxazole (SMX), bisphenol A (BPA) and methyl orange (MO). The selection of these target pollutants was based on the fact that they are frequently detected substances in aquatic environments and highly toxic to ecosystems (Zhang et al., 2015; Benotti et al., 2009; Sun et al., 2014). First, we fabricated the NPC materials by using direct carbonization of the MOF ([Zn₄O(BDC)₃], BDC = terephthalic acid). Second, following characterization of the morphology and pore structure, the adsorption kinetics and isotherms were investigated. Third, the adsorption capacities of the as-prepared NPC were evaluated in comparison with those of other promising adsorbents, i.e., single-walled carbon nanotubes (SWCNTs) and commercial powdered activated carbon (PAC). In addition, the adsorption properties of the three contaminants on NPC and the effect of pH were discussed. Based on these studies, a possible adsorption mechanism was elucidated.

1. Experimental

1.1. Materials and methods

MOF-5 was synthesized by using the methods described in a prior study (Zhao et al., 2011). Terephthalic acid (BDC) and zinc

nitrate hexahydrate were dissolved in diethylformamide, and then heated up to 130°C for 4 hr. After cooling down to room temperature, the solids were washed with acetone and dried at 60°C. The MOF-5 was carbonized directly to fabricate the NPC. Briefly, a quartz boat containing MOF-5 powder was placed into a vacuum tube furnace, where the samples were heated from room temperature to 1000°C under the protection of argon gas at the heating rate of 10°C/min. Then the temperature was maintained for 8 hr and the NPC was obtained after natural cooling under the protection of Ar gas.

Single-wall carbon nanotubes (SWCNTs, purchased from Chengdu Organic Chemicals Co., Ltd., China), were pretreated according to the methods reported by Lu and Chiu (2006). In brief, the SWCNTs were heated at 350°C for 30 min to remove the amorphous carbon, followed by purification using hydrochloric acid (HCl, 10 mol/L) to remove residual metal catalyst. Finally, the SWCNTs were washed with milli-Q water until the pH value was nearly neutral. Similarly, PAC (purchased from Sinopharm Chemical Reagent Co., Ltd., China) was pretreated by HCl (10 mol/L) and washed with Milli Q water before the adsorption experiments.

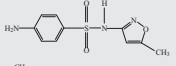
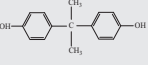
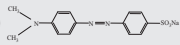
The stock solutions of SMX (98 wt%, J&K Chemical. Ltd.), BPA (96 wt%, J&K Chemical. Ltd.) and MO (96 wt%, Tianjin Damao Reagents Co.) with the concentration of 100 mg/L were prepared by dissolving the solids in Milli-Q water. Selected physicochemical properties of the contaminants are listed in Table 1.

1.2. Characterization and analyses

The morphology and pore structure of NPC were observed by using field emission scanning electron microscopy (FE-SEM, S-4800 Hitachi, Japan) and transmission electron microscopy (TEM, Tecnai G2 S-Twin, FEI, USA). The specific surface area was obtained by the multi-point Brunauer–Emmett–Teller (BET) method and calculated from the adsorption–desorption isotherms of N₂ at 77 K. The total pore volume (V_{total}) and micropore volume (V_{micro}) were calculated by the BJH method and derived from the V-t plot, respectively. The pore size distribution was calculated by the density functional theory (DFT) method. The chemical composition of NPC was measured by using X-ray photoelectron spectroscopy (XPS, Thermal ESCALAB 250, USA), implemented on a surface analysis system based on Al K α radiation. The powder X-ray diffraction measurement (XRD) was performed on a Rigaku D/MAX-2400 X-ray diffractometer. The Fourier transform infrared spectroscopy (FT-IR) spectra were recorded by a Vertex70, Bruker Vector FT-IR spectrometer. The Raman spectra were obtained by using a micro-Raman system 2000 spectrometer (Renishaw, UK), which was operated with He–Ne laser excitation. The Zeta potential of the adsorbents was measured at different pH values in 10 mM KCl solution by Zetasizer nano-ZS equipment (ZS 90, Malvern, UK). The solution pH was adjusted by HCl (1 mol/L) and NaOH (0.1 mol/L) prior to the measurements.

The concentrations of SMX and BPA were determined by a high-performance liquid chromatograph (HPLC, Waters

Table 1 – The physicochemical properties of SMX, BPA and MO.

Chemicals	Molecular size (Å)	Molecular weight (g/mol)	pK _a	Solubility (mg/L)
Sulfamethoxazole (SMX) 	13.3 × 4.7 × 3.8 (Ji et al., 2010)	253.27	1.8, 5.6 (Ji et al., 2010)	369.77 (Ji et al., 2010)
Bisphenol A (BPA) 	10.68 × 5.87 × 3.83 (Schafer et al., 2006)	228.29	9.6, 10.2 (Zheng et al., 2013)	120–300 (Zheng et al., 2013)
Methyl orange (MO) 	15.8 × 6.5 × 2.6 (Teng et al., 2012)	327.33	3.42 (Dutta and Dutta, 2014)	5000 (Kucukosmanoglu et al., 2006)

2695, Waters, USA) equipped with a C₁₈ column (15 cm × 4.6 mm × 5 μm) and a UV detector at a column temperature of 30°C. The flow rate was 1 mL/min. The SMX was determined at the wavelength of 265 nm with a mobile phase of acetonitrile containing 0.1% acetic acid solution (V:V = 40:60). The BPA was detected at the wavelength of 280 nm with a mobile phase of methanol:water (V:V = 70:30). The concentration of MO was measured by using a UV-visible spectrophotometer (UV7504, China).

1.3. Adsorption experiments

The batch adsorption experiments of SMX, BPA and MO were carried out in 50 mL quartz vessels containing 40 mL liquid volume of contaminant solutions. Two milligrams of adsorbent was added into each quartz vessel, which was sealed and placed in an orbital shaker with a rotation speed of 200 r/min at 20°C. The contaminant concentrations used in the kinetics and isotherm experiments were 15 mg/L and 10–100 mg/L, respectively. The initial solution pH values in the kinetics experiments were recorded as 5.8 (SMX), 6.0 (MO) and 6.3 (BPA), the change of which was negligible during the experiments. The contaminant amount adsorbed on adsorbents, q_t (mg/g), was calculated by Eq. (1):

$$q_t = \frac{(C_0 - C_t) \times V}{m} \quad (1)$$

where C_0 (mg/L) and C_t (mg/L) are the initial concentration of contaminants and the concentration at time t (min), respectively. V is the volume of the solution and m is the weight of the adsorbent.

In order to investigate the effect of pH, the adsorption experiments were carried out at initial concentrations of 30 mg/L for SMX and BPA while 50 mg/L for MO. The pH values of solutions were adjusted in the range of 2.0–11.0 by using HCl (1 mol/L) and NaOH (0.1 mol/L). The single-concentration point adsorption coefficient (K_d) was applied to represent the relative ratio of the contaminants adsorbed on NPC and in solution after reaching adsorption equilibrium, which was calculated as follows:

$$K_d = q_e / C_e \quad (2)$$

where q_e (mg/g) and C_e (mg/L) are the adsorbed amounts of the contaminant on the adsorbents and the concentration of contaminant in solution at equilibrium.

2. Results and discussion

2.1. Characterization of adsorbents

The SEM and TEM images of NPC are displayed in Fig. 1, and compared with those of SWCNTs and PAC. The NPC and MOF-5 exhibited the same cubic texture with a cube side length of 10 μm as shown in Fig. 1a and b, indicating that the carbonization process did not damage the morphology of the precursor. This result was in agreement with that reported by Pachfule et al. (2012). In addition, the pore structures on the NPC surface are clearly visible in Fig. 1c. Fig. 1d and e shows the morphology of the SWCNTs, which had a tubular texture with diameter of 10 nm. In comparison, the random structure of PAC can be observed in Fig. 1f.

The N₂ adsorption-desorption isotherms and pore distribution curves of MOF-5 and the three adsorbents are presented in Fig. 2. All the materials showed a type IV isotherm with hysteresis between the adsorption and desorption curves in the relative pressure range $P/P_0 = 0.4$ –1.0, indicating capillary condensation in the mesopores (Tang et al., 2015). The sharp rise at low relative pressure of $P/P_0 < 0.1$ for MOF-5, NPC and PAC suggested the existence of micropores. The almost vertical tail at P/P_0 near 1.0 for NPC indicated the presence of macroporosity (Liu et al., 2008; Li et al., 2015). The pore size distribution of NPC (Fig. 2b) displays a hierarchical porous structure with more meso- and macropores than PAC and SWCNTs, which accorded well with the V_{micro} and $V_{\text{meso/macro}}$ values (meso- and macroporous volume) listed in Table 2.

It is notable that MOF-5 presents a low special surface area of 151 m²/g, increasing dramatically to 1731 m²/g after carbonization. Generally, the solvent molecules on the MOF-5 surface occupied the pore channels after hydrothermal synthesis, causing the low surface area of 151 m²/g (Gonzalez et al., 2005; Liu et al., 2008). As the temperature increased in the carbonization process, all the solvent molecules were removed over 300°C, and subsequently, ZnO formed at temperatures higher than 425°C and was gradually reduced above 800°C. Finally, Zn metal (boiling point 908°C) vaporized away with the Ar flow, leaving carbon species alone in the NPC sample. (Liu et al., 2008; Chaikittisilp et al., 2013). As a result, NPC displays a high specific surface area of 1731 m²/g with a pore volume of 2.22 cm³/g, values higher than those of PAC (901 m²/g and 0.87 cm³/g) and SWCNTs (585 m²/g and 1.15 cm³/g). The typical survey spectra of XPS (Fig. 3(a)) show the presence of C and O elements in all the adsorbents. There

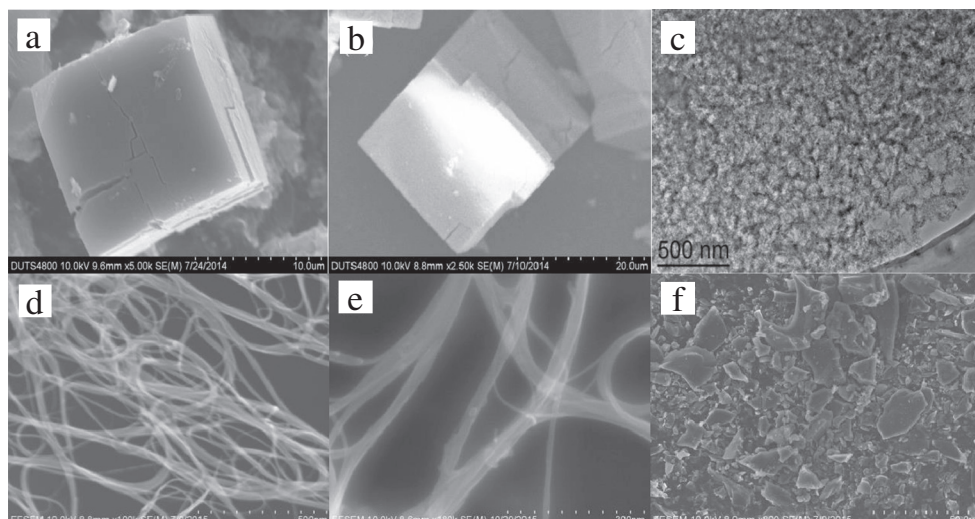


Fig. 1 – The scanning electron microscopy (SEM) images of (a) nanoporous carbon (NPC), (b) metal–organic framework-5 (MOF-5), (d, e) single-walled carbon nanotubes (SWCNTs), (f) powder active carbon (PAC) and transmission electron microscopy (TEM) image of NPC.

was no peak for Zn in NPC due to its evaporation from the carbon phase at 1000°C. Consequently, only the three elements of C (95.77%), O (2.98%) and N (1.25%) were determined in NPC. The XRD patterns of the three adsorbents reveal two broad peaks in the range 20–30° and 40–45° in Fig. 3b, corresponding to the (200) and (101) spacing of graphite, respectively. This result also confirmed the disappearance of Zn. In the Raman spectra, two obvious bands (D band at 1350 cm^{-1} and G band at 1580 cm^{-1}) were observed for NPC and PAC (Fig. 3c), demonstrating the co-existence of defects and a disordered structure as well as the graphitization of carbon (Hu et al., 2012). For the SWCNTs, however, only the G-band was observable, indicating a relatively ideal graphitized structure. The FT-IR spectra given in Fig. 3(d) indicate no essential differences among the three kinds of adsorbents. The characteristic bands at 3451 cm^{-1} , 1448 cm^{-1} and 1116 cm^{-1} should be ascribed to the stretching vibrations of –OH, C=C and C–O–C bonds, respectively. The strong band

at 1638 cm^{-1} indicates the characteristic C=C vibration of aromatic rings.

The zeta potential of NPC, SWCNTs and PAC tended to decline with increasing pH for all the adsorbents (Fig. 4). The pH_{iep} (the pH value where the zeta potential equals to zero) of NPC was observed to be 5.6, whereas the pH_{iep} for SWCNTs and PAC was 3.0 and 3.4, respectively.

2.2. Adsorption kinetics

The kinetics data of the three compounds' adsorption on NPC, SWCNTs and PAC were fitted best by the pseudo-second-order kinetics model (Fig. 5), with a higher correlation coefficient (R^2) relative to the pseudo-first-order model as shown in Table 3. The equations for modeling are presented as Eqs. (3) and (4). According to Fig. 5, adsorption equilibrium could be reached within the time of 10 hr for all of the contaminants. The most rapid adsorption took place in the first two hours, indicating

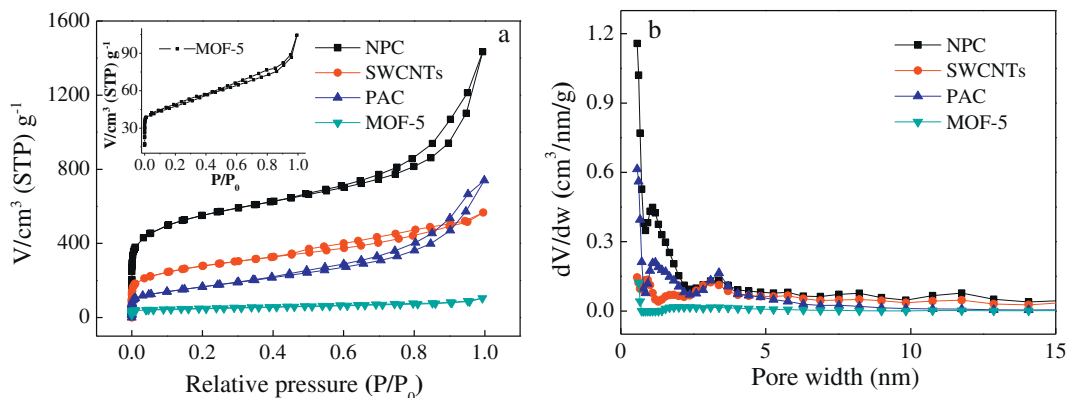


Fig. 2 – (a) N_2 adsorption–desorption isotherms and (b) pore distribution curves of MOF-5, NPC, SWCNTs and PAC.

Table 2 – Selected physicochemical parameters of adsorbents.

Samples	S_{BET} (m^2/g)	V_{total} (cm^3/g)	$V_{\text{meso/macro}}$ (cm^3/g)	V_{micro} (cm^3/g)	D_{average} (nm)
MOF-5	151	0.16	0.11	0.05	4.29
NPC	1731	2.22	1.68	0.54	4.77
SWCNTs	585	1.15	1.12	0.03	7.83
PAC	901	0.87	0.65	0.22	3.90

S_{BET} : Special surface area; V_{total} : total volume; $V_{\text{meso/macro}}$: meso- and macroporous volume; D_{average} : average diameter.

a fast initial transfer of contaminants to the surface of the adsorbents.

Pseudo-first-order kinetics model: $\ln(q_e - q_t) = \ln q_e - k_1 t$ (3)

Pseudo-second-order kinetics model: $\frac{t}{q_t} = \frac{1}{k_2 q_e^2} + \frac{1}{q_e} t$ (4)

$$= \frac{1}{v_o} + \frac{t}{q_e}$$

where q_t and q_e (mg/g) are the adsorbed amounts of the contaminants on the adsorbents at time t (hr) and equilibrium respectively. k_1 (1/hr) and k_2 (g/mg/hr) are the adsorption rate constants of the pseudo-first-order and pseudo-second-order models. v_o (mg/hr/g) is the initial adsorption rate.

To identify the crucial diffusion step, the kinetics data were simulated by the intra-particle diffusion model (Eq. (5)) developed by McKay and Poots (1980):

$$q_t = k_d t^{1/2} \quad (5)$$

where q_t (mg/g) is the amount of contaminant adsorbed on the adsorbents at time t (hr), and k_d (mg/g/hr^{1/2}) is the adsorption rate constant related to the intraparticle diffusivity.

The adsorption could be divided into three stages, i.e., external diffusion, intra-particle diffusion and the adsorption of adsorbates onto the active sites. In general, the last stage is a rapid process, and hence the first two stages are proposed to be the limiting steps that determine the overall adsorption rate. As

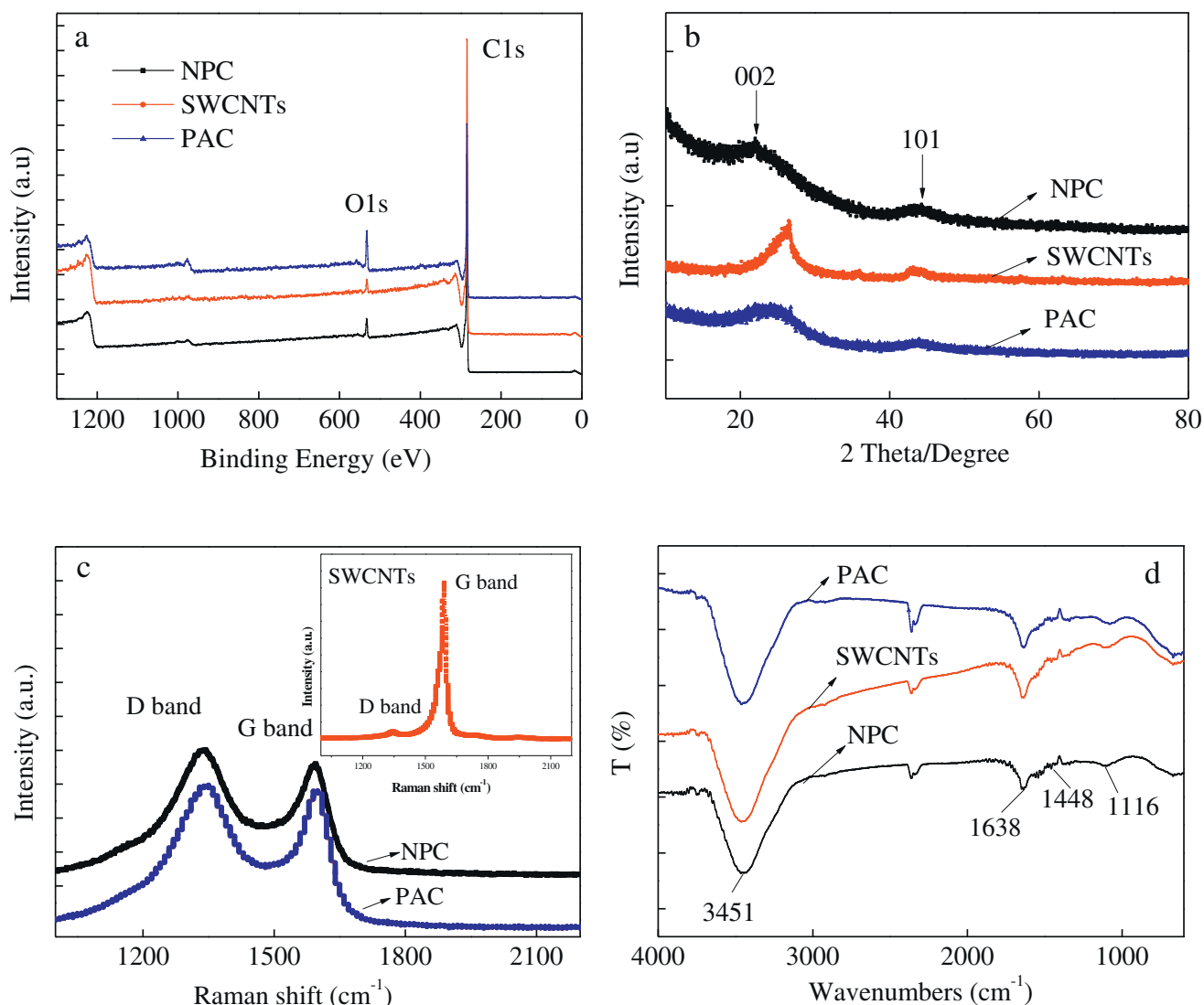


Fig. 3 – (a) X-ray photoelectron spectroscopy (XPS) survey spectra, (b) X-ray diffraction measurement (XRD) pattern, (c) Raman spectra and (d) FT-IR spectra of NPC, SWCNTs and PAC.

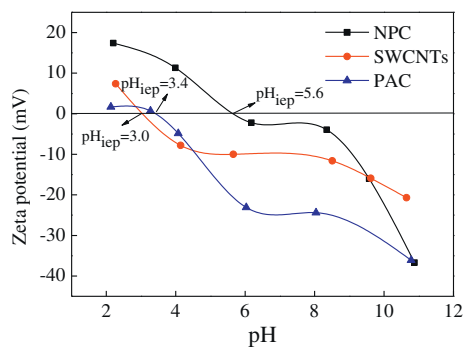


Fig. 4 – Zeta potential as a function of pH for NPC, SWCNTs and PAC.

shown in Fig. 6, all the plots of uptake (q_t) versus the square root of time ($t^{1/2}$) appear to be the nonlinear and do not pass the origin, which is indicative of some degree of boundary layer control. Thus, the intra-particle diffusion should not be the only

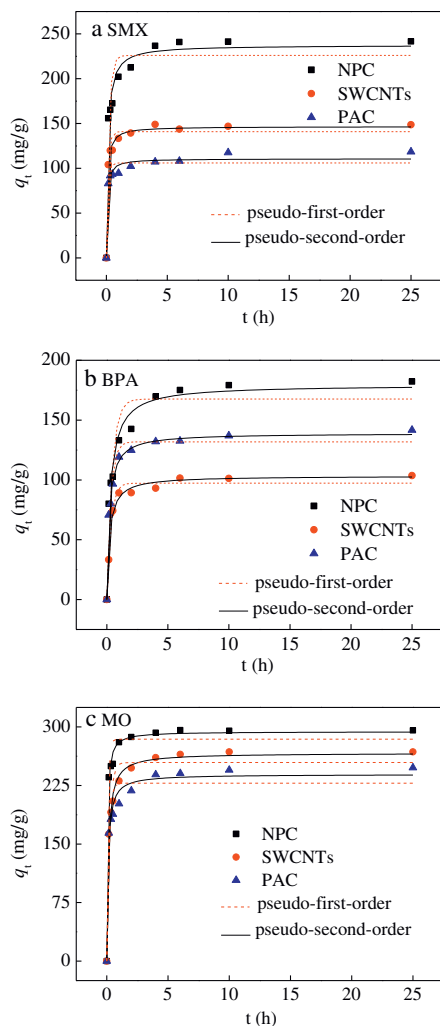


Fig. 5 – The adsorption capacity of (a) sulfamethoxazole (SMX), (b) Bisphenol A (BPA) and (c) methyl orange versus time (t) fitted by pseudo-first-order and pseudo-second-order models.

rate-limiting step (Allison, 2007). For all the adsorbents, the initial segment of the plot presents a greater slope than that of the second segment, as shown in Table 4, which followed the order of $MO > SMX > BPA$. This indicated the more rapid transfer of MO molecules from bulk solution and passing through the boundary layer of the adsorbent surface compared with that of SMX and BPA. Consequently, MO presents the largest adsorption rate (v_0) (Table 3). On the other hand, the K_{d1} value of SWCNTs for MO and SMX is higher than that of NPC and PAC (Table 4). This means that the adsorbates may easily diffuse into the inner pores of SWCNTs (Yu et al., 2009). It is inferred that the relatively large pore size of SWCNTs should be responsible for the rapid intraparticle diffusion of the adsorbates, resulting in the higher K_{d1} value.

2.3. Adsorption isotherms

Fig. 7 illustrates the adsorption isotherms fitted by the well-known Langmuir and Freundlich models, which are listed as below:

$$\text{Langmuir model: } q_e = \frac{b q_m C_e}{1 + b C_e} \quad (6)$$

$$\text{Freundlich model: } q_e = K_F C_e^n \quad (7)$$

where q_m (mg/g) is the maximum adsorption capacity of the adsorbents, and b is the Langmuir constant related to adsorption energy; K_F and n are the Freundlich constants associated with the adsorption capacity and adsorption intensity of the adsorbents.

Compared with the Freundlich model, the Langmuir model for NPC adsorption provided a better fit to all the experimental data, with $R^2 \geq 0.984$ (Table 5). This strongly indicated the possible occurrence of monolayer adsorption (Caliskan and Gokturk, 2010; Yu et al., 2009). On the other hand, multilayer adsorption might also take place at an increased equilibrium concentration because of the hydrogen bonding and π -electron polarization between contaminant molecules (Caliskan and Gokturk, 2010). In addition, all the isotherms were nonlinear because the fitted n values of the Freundlich model varied over the range of 0.15–0.57. This implied the presence of heterogeneous adsorption sites on the adsorbent surface in association with the involvement of oxygen-containing groups on the NPC surface (Fig. 3d).

The NPC demonstrated a higher adsorption capacity towards the three kinds of contaminants than both SWCNTs and PAC. As shown in Table 5, the q_m values for SMX, BPA and MO on NPC were 625 mg/g, 757 mg/g and 872 mg/g respectively, 1.02–3.23 times higher than those on SWCNTs and PAC. In addition, the NPC also presents higher adsorption capacity than those reported in previous studies. For example, the adsorption capacity of activated carbon towards SMX was 185.19 mg/g as reported by Caliskan and Gokturk (2010), while the q_m values of biochar towards SMX were lower than 10 mg/g (Sun et al., 2016). For BPA, the adsorption capacity on SWCNTs was reported to be 199 mg/g in Liu's work (Liu et al., 2014), while the q_m value of MO adsorption on MOF-235 calculated by Haque et al. (2011) was 477 mg/g. Taken together, these compounds exhibit the largest q_m values for adsorption on the NPC.

Table 3 – Summary of parameters for adsorption of SMX, BPA and MO on three adsorbents fitted by pseudo-first-order and pseudo-second-order models.

Compound	Adsorbent	Pseudo-first-order model			Pseudo-second-order model		
		k_1 (1/hr)	R^2	q_e (mg/g)	v_0 (mg/hr/g)	k_2 (g/mg/hr)	R^2
SMX	NPC	4.76	0.9185	237.5	1979.2	0.035	0.9745
	SWCNTs	6.98	0.9652	146.6	1954.5	0.090	0.9934
	PAC	8.14	0.9396	110.6	1627.1	0.13	0.9739
BPA	NPC	2.34	0.9236	179.4	618.6	0.019	0.9769
	SWCNTs	3.17	0.9726	103.4	492.4	0.046	0.9741
	PAC	3.17	0.9624	139.0	595.0	0.031	0.9908
MO	NPC	5.99	0.9247	294.1	5994.1	0.069	0.9937
	SWCNTs	9.54	0.9693	266.7	2205.0	0.031	0.9938
	PAC	4.72	0.9531	239.2	2460.3	0.043	0.9780

2.4. Influencing factors of adsorption

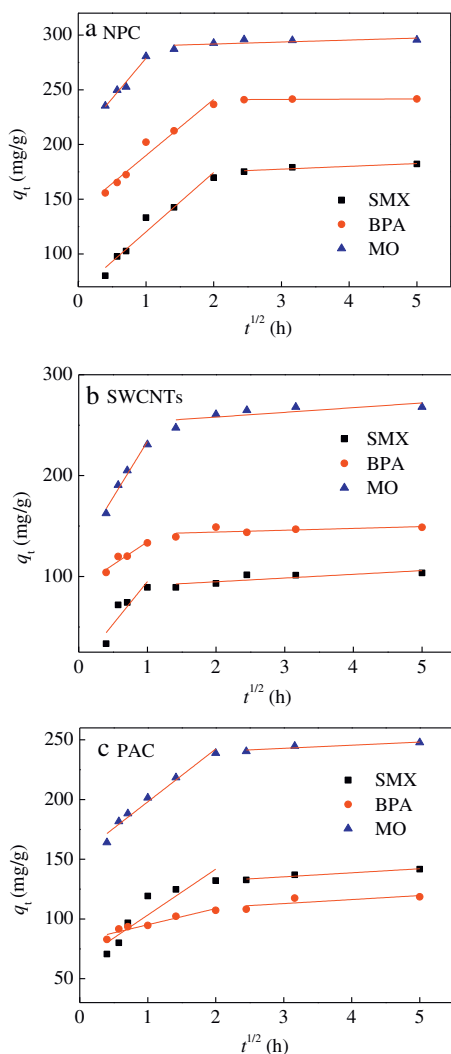
The specific surface area should constitute the most important factor having a crucial impact on the adsorption capacity of a specific adsorbent. As shown in Table 2, NPC possesses

the highest S_{BET} value (1731 m²/g) compared with PAC (901 m²/g) and SWCNTs (585 m²/g). In addition, the meso/macroporous volume (1.68 cm³/g) accounted for 76% of the total pore volume (V_{total}) for NPC, higher than the V_{total} values of SWCNTs (1.15 cm³/g) and PAC (0.87 cm³/g). This unique property of NPC should be responsible for its possession of the highest adsorption capacity observed here.

Among all the investigated compounds, despite the lower hydrophobicity of MO, its adsorption capacity on NPC was higher than that of BPA and SMX. For NPC, the micropores accounted for 24% of the pore volume (Table 2), with the peak in the distribution at 1.1 nm, as presented in Fig. 2b. For the cylindrical or ellipsoidal pores of NPC, it is the second-widest dimension of an adsorbate molecular that determines its accessibility to the pores; while for slit-shaped pores, the smallest dimension of the pollutant molecule is the determining factor (Zhang et al., 2010). Therefore, the pore-filling mechanism would affect these compounds' adsorption owing to their second-widest dimension being lower than 1.1 nm (Table 1) (Ji et al., 2010; Dubinin, 1975; Ismadji and Bhatia, 2001). Moreover, it is notable that π -electron polarization and hydrogen bonding could also occur between contaminant molecules or between the adsorbents and contaminants. However, the electrostatic interaction does not appear likely to influence the adsorption under the experimental pH values (5.8 for SMX, 6.3 for BPA and 6.0 for MO) because of the pH_{iep} value 5.6 for NPC. Therefore, the q_m sequence of MO > BPA > SMX is a consequence of the collective contribution of pore-filling mechanism, π -electron polarization and hydrogen bonding.

2.5. Effect of pH values

Fig. 8 reveals the effects of pH on NPC adsorption towards SMX, BPA and MO. The adsorption patterns of SMX, BPA and MO behaved in a quite different manner when the solution pH varied

**Fig. 6 – Plot of intra-particle diffusion model for adsorption of three contaminants on (a) NPC, (b) SWCNTs and (c) PAC.****Table 4 – Parameters for intra-particle diffusion model.**

Compound	K_{d1} (mg/g/hr ^{1/2})		
	NPC	SWCNTs	PAC
BPA	51.26	45.41	13.54
SMX	54.29	84.31	38.40
MO	73.52	111.02	44.21

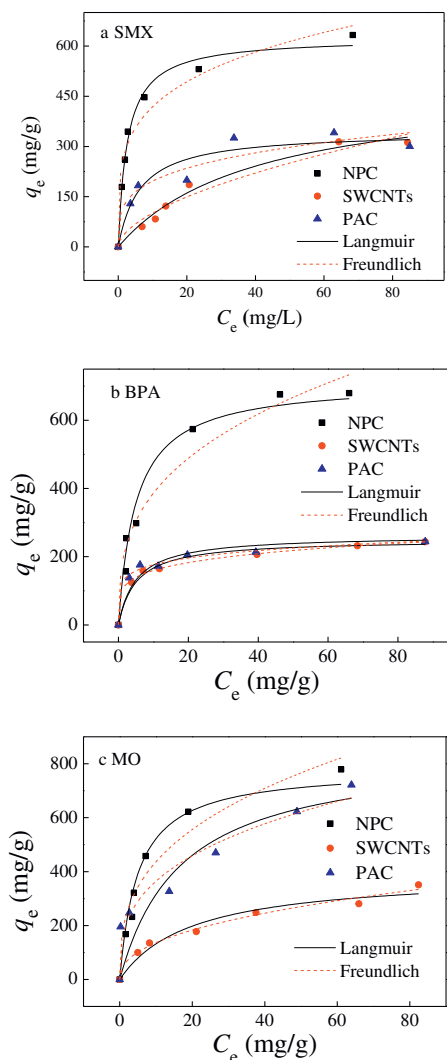


Fig. 7 – Adsorption isotherms of (a) SMX, (b) BPA, (c) MO on different adsorbents fitted by Langmuir and Freundlich equations.

from 2.0 to 11.0. For SMX, the maximum K_d value was obtained at pH 4. Taking into account the pK_a values of 1.8 and 5.6 for SMX (Table 1), the zwitterionic molecules of SMX ($SMX^{+/-}$) were dominant in the pH range of 1.8–5.6, thus the electrostatic repulsion was enhanced between the protonated amino group of

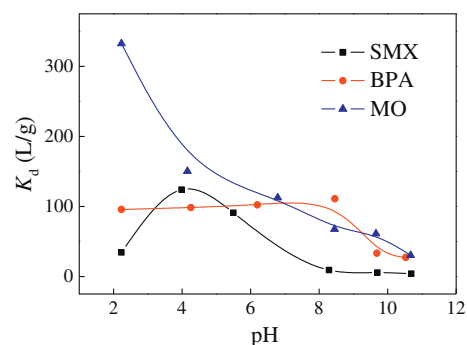


Fig. 8 – Effect of pH on K_d values of SMX, BPA and MO adsorption on NPC.

SMX and positively charged NPC at pH < 1.8. Moreover, the electrostatic repulsion increased between SMX anion (SMX^-) and negatively charged NPC at pH > 5.6. Therefore, the highest K_d value occurred at pH 4. On the other hand, the BPA molecule is the dominant species at pH lower than the pK_{a1} of 9.6. Thus, the K_d value decreased at pH > 9.6 due to the electrostatic repulsion between BPA^- and negatively charged NPC. For MO adsorption at $pK_a(MO) < pH < pK_{iep}$, the electrostatic attraction was weakened between MO^- and positively charged NPC as the pH increased. Moreover, the electrostatic repulsion was strengthened between MO^- and negatively charged NPC at pH > pK_{iep} . Hence, it is not surprising to observe a decreased K_d value in the pH range of 2–11. These results clearly indicate the important contribution of electrostatic interaction in the adsorption of the three contaminants on NPC.

3. Conclusions

The MOF-5-derived NPCs possessed a high specific surface area of 1731 m^2/g and a high proportion of meso/macropore volume of 1.68 cm^3/g . NPC was shown to have a high adsorption capacity of 625, 757 and 872 mg/g respectively towards SMX, BPA and MO, 1.02–3.23 times higher than those of SWCNTs and commercial PAC. Notably, MO had the largest adsorption rate among the three compounds for NPC adsorption, resulting from the rapid transfer of MO molecules from bulk solution to the boundary of the NPC surface. Moreover, the fact that NPC exhibited the highest adsorption capacity towards MO suggested the significant role of adsorbent and

Table 5 – Summary of parameters for isotherm models for adsorption of SMX, BPA and MO on different adsorbents.

Compound	Adsorbent	Langmuir constants		Freundlich constants		
		q_m (mg/g)	R^2	K_F ($mg^{(1-n)}L^n/g$)	n	R^2
SMX	NPC	625 ± 20.3	0.988	242 ± 24.0	0.24 ± 0.03	0.957
	SWCNTs	484 ± 47.3	0.980	27.4 ± 7.88	0.57 ± 0.07	0.955
	PAC	344 ± 30.9	0.912	108 ± 26.2	0.26 ± 0.06	0.902
BPA	NPC	757 ± 33.1	0.984	177 ± 28.8	0.34 ± 0.05	0.958
	SWCNTs	242 ± 8.59	0.980	102 ± 4.02	0.19 ± 0.01	0.996
	PAC	234 ± 9.82	0.973	124 ± 7.03	0.15 ± 0.02	0.988
MO	NPC	872 ± 32.4	0.991	195 ± 30.7	0.35 ± 0.05	0.942
	SWCNTs	394 ± 40.6	0.955	51.2 ± 7.14	0.43 ± 0.04	0.985
	PAC	850 ± 216	0.816	170 ± 36.2	0.33 ± 0.06	0.945

contaminant interactions, such as the pore-filling mechanism and electrostatic interaction. The surface area and pore structure of carbonaceous adsorbents should be of particular importance in removal of contaminants from aqueous solution. By virtue of several unique advantages, the MOF-derived NPC shows considerable potential as an effective adsorbent for water and wastewater treatment.

Acknowledgements

This work was supported by the National Natural Science Foundation of China (Nos. 21437001 and 21407019) and Open Project of State Key Laboratory of Urban Water Resource and Environment, Harbin Institute of Technology (No. QA201617).

REFERENCES

- Allison, A.L., 2007. Hazardous Materials and Wastewater: Treatment, Removal and Analysis. Nova Science Publishers, Inc., New York.
- Alsaiee, A., Smith, B.J., Xiao, L., Ling, Y., Helbling, D.E., Dichtel, W.R., 2016. Rapid removal of organic micropollutants from water by a porous beta-cyclodextrin polymer. *Nature* 529 (7585), 190–194.
- Bedin, K.C., Martins, A.C., Cazetta, A.L., Pezoti, O., Almeida, V.C., 2016. KOH-activated carbon prepared from sucrose spherical carbon: adsorption equilibrium, kinetic and thermodynamic studies for methylene blue removal. *Chem. Eng. J.* 286, 476–484.
- Benotti, M.J., Trenholm, R.A., Vanderford, B.J., Holady, J.C., Stanford, B.D., Snyder, S.A., 2009. Pharmaceuticals and endocrine disrupting compounds in US drinking water. *Environ. Sci. Technol.* 43 (3), 597–603.
- Byun, J., Patel, H.A., Thirion, D., Yavuz, C.T., 2016. Charge-specific size-dependent separation of water-soluble organic molecules by fluorinated nanoporous networks. *Nat. Commun.* 7, 13377.
- Caliskan, E., Gokturk, S., 2010. Adsorption characteristics of sulfamethoxazole and metronidazole on activated carbon. *Sep. Sci. Technol.* 45 (2), 244–255.
- Chaikittisilp, W., Hu, M., Wang, H., Huang, H.S., Fujita, T., Wu, K.C.W., 2012. Nanoporous carbons through direct carbonization of a zeolitic imidazolate framework for supercapacitor electrodes. *Chem. Commun.* 48 (58), 7259–7261.
- Chaikittisilp, W., Ariga, K., Yamauchi, Y., 2013. A new family of carbon materials: synthesis of MOF-derived nanoporous carbons and their promising applications. *J. Mater. Chem. A* 1 (1), 14–19.
- Dubinin, M.M., 1975. Porous structure and adsorption properties of activated carbons. In: Walker, P.L. (Ed.), *Chemistry and Physics of Carbon*. vol. 2. Marcel Dekker, New York, p. 51e120.
- Dutta, A., Dutta, R.K., 2014. Fluorescence behavior of cis-methyl orange stabilized in cationic premicelles. *Spectrochim. Acta A-Molec. Biomol. Spectrosc.* 126, 270–279.
- Gadipelli, S., Patel, H.A., Guo, Z., 2015. An ultrahigh pore volume drives up the amine stability and cyclic CO₂ capacity of a solid-amine@carbon sorbent. *Adv. Mater.* 27 (33), 4903–4909.
- Gonzalez, J., Devi, R.N., Tunstall, D.P., Cox, P.A., Wright, P.A., 2005. Deuterium NMR studies of framework and guest mobility in the metal-organic framework compound MOF-5, Zn₄O(O₂CC₆H₄CO₂)₃. *Microporous Mesoporous Mater.* 84 (1–3), 97–104.
- Haque, E., Jun, J.W., Jhung, S.H., 2011. Adsorptive removal of methyl orange and methylene blue from aqueous solution with a metal-organic framework material, iron terephthalate (MOF-235). *J. Hazard. Mater.* 185 (1), 507–511.
- Hu, J., Wang, H., Gao, Q., Guo, H., 2010. Porous carbons prepared by using metal-organic framework as the precursor for supercapacitors. *Carbon* 48 (12), 3599–3606.
- Hu, M., Reboul, J., Furukawa, S., Torad, N.L., Ji, Q., Srinivasu, P., Ariga, K., Kitagawa, S., Yamauchi, Y., 2012. Direct carbonization of Al-based porous coordination polymer for synthesis of nanoporous carbon. *J. Am. Chem. Soc.* 134 (6), 2864–2867.
- Ismadji, S., Bhatia, S.K., 2001. A modified pore-filling isotherm for liquid-phase adsorption in activated carbon. *Langmuir* 17 (5), 1488–1498.
- Ji, L., Liu, F., Xu, Z., Zheng, S., Zhu, D., 2010. Adsorption of pharmaceutical antibiotics on template-synthesized ordered micro- and mesoporous carbons. *Environ. Sci. Technol.* 44 (8), 3116–3122.
- Kim, B.J., Park, S.J., 2007. Influence of surface treatments on micropore structure and hydrogen adsorption behavior of nanoporous carbons. *J. Colloid Interface Sci.* 311 (2), 619–621.
- Kucukosmanoglu, M., Gezici, O., Ayar, A., 2006. The adsorption behaviors of methylene blue and methyl orange in a diaminoethanesporopollenin-mediated column system. *Sep. Purif. Technol.* 52 (2), 280–287.
- Lee, H.J., Cho, W., Lim, E., Oh, M., 2014. One-pot synthesis of magnetic particle-embedded porous carbon composites from metal-organic frameworks and their sorption properties. *Chem. Commun.* 50 (41), 5476–5479.
- Li, X., Chen, S., Fan, X., Quan, X., Tan, F., Zhang, Y., Gao, J., 2015. Adsorption of ciprofloxacin, bisphenol and 2-chlorophenol on electrospun carbon nanofibers: in comparison with powder activated carbon. *J. Colloid Interface Sci.* 447, 120–127.
- Li, M., Wang, J., Jiao, C., Wang, C., Wu, Q., Wang, Z., 2016. Magnetic porous carbon derived from a Zn/Co bimetallic metal-organic framework as an adsorbent for the extraction of chlorophenols from water and honey tea samples. *J. Sep. Sci.* 39 (10), 1884–1891.
- Lim, S., Suh, K., Kim, Y., Yoon, M., Park, H., Dybtsev, D.N., Kim, K., 2012. Porous carbon materials with a controllable surface area synthesized from metal-organic frameworks. *Chem. Commun.* 48 (60), 7447–7449.
- Liu, B., Shioyama, H., Akita, T., Xu, Q., 2008. Metal-organic framework as a template for porous carbon synthesis. *J. Am. Chem. Soc.* 130 (16), 5390.
- Liu, F.F., Zhao, J., Wang, S., Du, P., Xing, B., 2014. Effects of solution chemistry on adsorption of selected pharmaceuticals and personal care products (PPCPs) by graphenes and carbon nanotubes. *Environ. Sci. Technol.* 48 (22), 13197–13206.
- Lu, C.Y., Chiu, H.S., 2006. Adsorption of zinc(II) from water with purified carbon nanotubes. *Chem. Eng. Sci.* 61 (4), 1138–1145.
- McKay, G., Poots, V.J.P., 1980. Kinetics and diffusion-processes in color removal from effluent using wood as an adsorbent. *J. Chem. Technol. Biotechnol.* 30 (6), 279–292.
- Pachfule, P., Biswal, B.P., Banerjee, R., 2012. Control of porosity by using isoreticular zeolitic imidazolate frameworks (IRZIFs) as a template for porous carbon synthesis. *Chem.-A Eur. J.* 18 (36), 11399–11408.
- Patel, H.A., Bajaj, H.C., Jasra, R.V., 2009. Sorption of nitrobenzene from aqueous solution on organoclays in batch and fixed-bed systems. *Ind. Eng. Chem. Res.* 48 (2), 1051–1058.
- Prehal, C., Koczwar, C., Jaekel, N., Schreiber, A., Burian, M., Amenitsch, H., Hartmann, M.A., Presser, V., Paris, O., 2017. Quantification of ion confinement and desolvation in nanoporous carbon supercapacitors with modelling and in situ X-ray scattering. *Nat. Energy* 2 (3), 16215.
- Schafer, A.I., Nghiem, L.D., Oschmann, N., 2006. Bisphenol A retention in the direct ultrafiltration of greywater. *J. Membr. Sci.* 283 (1–2), 233–243.

- Seo, J.S., Whang, D., Lee, H., Jun, S.I., Oh, J., Jeon, Y.J., Kim, K., 2000. A homochiral metal-organic porous material for enantioselective separation and catalysis. *Nature* 404 (6781), 982–986.
- Sneddon, G., Greenaway, A., Yiu, H.P., 2014. The potential applications of nanoporous materials for the adsorption, separation, and catalytic conversion of carbon dioxide. *Adv. Energy Mater.* 4 (10), 1301873.
- Sun, Y., Wang, G., Dong, Q., Qian, B., Meng, Y., Qiu, J., 2014. Electrolysis removal of methyl orange dye from water by electrospun activated carbon fibers modified with carbon nanotubes. *Chem. Eng. J.* 253, 73–77.
- Sun, B., Lian, F., Bao, Q., Liu, Z., Song, Z., Zhu, L., 2016. Impact of low molecular weight organic acids (LMWOAs) on biochar micropores and sorption properties for sulfamethoxazole. *Environ. Pollut.* 214, 142–148.
- Tang, J., Salunkhe, R.R., Liu, J., Torad, N.L., Imura, M., Furukawa, S., Yamauchi, Y., 2015. Thermal conversion of core-shell metal-organic frameworks: a new method for selectively functionalized nanoporous hybrid carbon. *J. Am. Chem. Soc.* 137 (4), 1572–1580.
- Teng, M., Qiao, J., Li, F., Bera, P.K., 2012. Electrospun mesoporous carbon nanofibers produced from phenolic resin and their use in the adsorption of large dye molecules. *Carbon* 50 (8), 2877–2886.
- Uner, O., Gecgel, U., Bayrak, Y., 2016. Adsorption of methylene blue by an efficient activated carbon prepared from *Citrus aurantium* rind: kinetic, isotherm, thermodynamic, and mechanism analysis. *Water Air Soil Pollut.* 227 (7), 247.
- Yang, S.J., Kim, T., Im, J.H., Kim, Y.S., Lee, K., Jung, H., Park, C.R., 2012. MOF-derived hierarchically porous carbon with exceptional porosity and hydrogen storage capacity. *Chem. Mater.* 24 (3), 464–470.
- Yu, Q., Zhang, R., Deng, S., Huang, J., Yu, G., 2009. Sorption of perfluorooctane sulfonate and perfluorooctanoate on activated carbons and resin: kinetic and isotherm study. *Water Res.* 43 (4), 1150–1158.
- Zhang, S., Shao, T., Kose, H.S., Karanfil, T., 2010. Adsorption of aromatic compounds by carbonaceous adsorbents: a comparative study on granular activated carbon, activated carbon fiber, and carbon nanotubes. *Environ. Sci. Technol.* 44 (16), 6377–6383.
- Zhang, Q.Q., Ying, G.G., Pan, C.G., Liu, Y.S., Zhao, J.L., 2015. Comprehensive evaluation of antibiotics emission and fate in the river basins of China: source analysis, multimedia modeling, and linkage to bacterial resistance. *Environ. Sci. Technol.* 49 (11), 6772–6782.
- Zhao, Z., Ma, X., Li, Z., Lin, Y.S., 2011. Synthesis, characterization and gas transport properties of MOF-5 membranes. *J. Membr. Sci.* 382 (1–2), 82–90.
- Zheng, S., Sun, Z., Park, Y., Ayoko, G.A., Frost, R.L., 2013. Removal of bisphenol A from wastewater by Ca-montmorillonite modified with selected surfactants. *Chem. Eng. J.* 234, 416–422.